Applied Geochemistry 131 (2021) 105045

Contents lists available at ScienceDirect

Applied Geochemistry

journal homepage: www.elsevier.com/locate/apgeochem

Potential impact of cementitious leachates on the buffer porewater chemistry in the Finnish repository for spent nuclear fuel – A reactive transport modelling assessment

Marek Pekala [a,*,1], Paul Wersin [a], Barbara Pastina [b], Ralf Lamminmäki [b], Marja Vuorio [c], Andreas Jenni [a]

[a] Rock-Water Interaction, Institute of Geological Sciences, University of Bern, Baltzerstrasse 1+3, 3012, Bern, Switzerland
[b] Posiva Oy, Olkiluoto, 27160, Eurajoki, Finland
[c] COVRA N.V., Postbus 202, 4380 AE, Vlissingen, Netherlands

ARTICLE INFO

Keywords:
Geological repository for spent nuclear fuel in Finland
Bentonite buffer porewater composition
Cement leachates
Reactive transport modelling
Performance and safety assessment

ABSTRACT

Cementitious materials will be used during the construction and operation of a geological repository for spent nuclear fuel at Olkiluoto in Finland. Upon contacting water, cement dissolution will generate high-pH leachates, which might eventually reach the proximity of a canister deposition hole through an interconnected network of fractures in the crystalline host rock. Highly-alkaline conditions near the bentonite buffer surrounding the canister could affect the performance of the buffer safety functions. In this study, we evaluate the potential impact such cement leachates might have on the chemical composition of the buffer porewater over time-frames relevant for the safety assessment of the repository.

Although a comprehensive mechanistic assessment of these interactions is not possible due to their complexity, we demonstrate that key processes and their impact on the chemical composition of the bentonite porewater can be bounded. To this end we apply a reactive transport modelling based on an analysis of processes and parameter values. The model considers a 3D geometry including: the canister, the bentonite buffer, and a discrete fracture in the rock intersecting the deposition hole. Cement leachates flow through the fracture around the deposition hole, while solutes exchange with the buffer porewater *via* advective and diffusive mass transfer.

Modelling results indicate that a combination of restricted water flow within the fracture, slow diffusive solute transport in the buffer, and chemical reactions will act together to minimise the extent of buffer porewater perturbation, should cement leachates reach the vicinity of a deposition hole. The model pessimistically estimates a maximum pH variation to be below 0.1 unit, and a maximum concentration change of about factor 3 (relative to initial) for reacting components within most of the buffer volume. This is only about double the perturbation values predicted for "natural" evolution of the buffer porewater, in the absence of cement leachates.

Model uncertainties are evaluated by a series of sensitivity cases. These calculations suggest that additional processes, not directly accounted for in the base model (such as leachate-groundwater mixing and dilution on transport through the fracture network, and porosity reduction in the buffer due to mineral precipitation), could significantly contribute to a further reduction of the magnitude of potential buffer porewater perturbation.

1. Introduction

POSIVA (www.posiva.fi), the Finnish radioactive waste management company, considers disposing of spent nuclear fuel in the Olkiluoto crystalline bedrock at a depth of 400–450 m (POSIVA, 2012a). According to the adopted multiple-barrier disposal concept, spent nuclear fuel will be packed in canisters made of copper and cast iron. Tunnels will be excavated inside the rock, and the canisters will be placed in holes drilled within the tunnels. Remaining cavities will be filled with bentonite-based clay to provide favourable physical and

* Corresponding author.
E-mail address: marek.pekala@bfe.bund.de (M. Pekala).
[1] Currently at the Federal Office for the Safety of Nuclear Waste Management (Bundesamt für die Sicherheit der nuklearen Entsorgung – BASE), 11513 Berlin, Germany.

https://doi.org/10.1016/j.apgeochem.2021.105045
Received 29 March 2021; Received in revised form 8 June 2021; Accepted 25 June 2021
Available online 7 July 2021

chemical conditions near the canister (POSIVA, 2012a). Fig. 1 schematically illustrates the KBS-V disposal concept, whereby disposal packages are deposited in vertical deposition holes drilled from horizontal deposition tunnels.

Cementitious materials of various types and quantities (used for rock stabilisation, to limit groundwater inflow, for sealing of the deposition tunnels, and for the construction of other engineering structures) will be present in the repository after closure (POSIVA, 2012b). Although the buffer will not be in direct contact with cementitious materials, it may be exposed to cementitious fluids derived from cement leaching occurring at other locations within and near the repository, transported through an interconnected network of fractures in the rock by flowing groundwater.

The suitability of the Olkiluoto bedrock for final disposal of spent nuclear fuel is demonstrated with a so-called safety case (POSIVA, 2012a). An integral part of the safety case is a detailed analysis of potential failure modes of the engineered barrier system, and the long-term consequences of such events. For example, should a disposal canister fail after repository closure, the rate of radionuclide release will be affected by the chemical conditions in the bentonite buffer, which define radionuclide solubility, sorption and transport. Repository safety calculations considered several possible groundwater compositions (Hellä et al., 2014). A High-Alkaline Bounding Groundwater was defined to represent the potential effect of high-pH solutions originating from the leaching of cementitious materials left in the repository after closure. The composition of this water was approximated by imposing pH of 10 (simplistically representing an expected extensive period after complete portlandite dissolution during which Calcium Silicate Hydrate phases control cement water pH) on the Saline Reference Groundwater (Hellä et al., 2014). Based on thus calculated composition of the High-Alkaline Bounding Groundwater, the corresponding composition of the buffer porewater was defined by performing batch thermochemical equilibrium calculations. The so calculated pH value for the buffer porewater is however uncertain because various complex processes expected to take place during these interactions are either treated simplistically or neglected altogether. These uncertainties are subsequently propagated into later phases of safety analysis, e.g. the evaluation of radionuclide solubility, retardation and transport.

An assessment of the potential impact of cementitious materials left in the repository after closure, on the integrity of the bentonite buffer, has been carried out within POSIVA's programme utilising a variety of approaches (e.g. Vieno et al., 2003; Montori et al., 2008; Lehikoinen, 2009; Soler, 2010; Soler, 2011a; Soler et al., 2011b; Soler, 2012; Koskinen, 2013). These studies focused on various aspects related with the chemical and mechanical stability of the bentonite buffer, such as the extent of montmorillonite dissolution, buffer stability, porosity changes, mineralogical alteration and cementation processes. However, to date no systematic study has been carried out with the specific focus on the potential perturbation of the buffer porewater chemistry.

The objective of this paper is to bound the extent to which the buffer porewater chemical composition could be altered due to interactions with cement leachates over timescales relevant from the safety assessment point of view. To address this problem, a reactive transport modelling methodology is used.

Lehikoinen (2009) performed reactive transport calculations to shed light on the possible extent of mineralogical alteration of the bentonite buffer due to alkaline plume originating from degrading cementitious materials at Olkiluoto. Most of the calculations were carried out utilising a simplified 1D model geometry. Importantly, in the 1D model geometry a fixed composition transport boundary condition was applied on the exterior surface of the buffer. This is a simplifying and conservative modelling choice (infinite cement leachate reservoir in contact with the bentonite buffer), which tends to exaggerate the impact of the cement leachates on the buffer. Based on preliminary scoping calculations, Lehikoinen (2009) proposed that reactive transport calculations performed over a 2D geometry are needed to gain a more comprehensive view of the bentonite buffer alterations.

In the present paper, for the first time, calculations are performed over a 3D geometry of the deposition hole, explicitly accounting for the flow of cement leachates within a discrete fracture intersecting the deposition hole. Such geometry definition allows for the mass transfer between the fracture and the buffer to be represented more realistically. In particular, the effect of a mixing zone between the buffer porewater and the cement leachates is represented more accurately. In addition, the finite volume of the fracture means that its capacity to supply cement leachates towards the buffer, and its capacity to receive bentonite porewater solutes is likewise finite. Both the above constitute a significant improvement over an arbitrary definition of a fixed composition boundary condition. The model is implemented in the PFLOTRAN code.

The results of this work can be used as a basis for evaluating the potential impact of cement leachates on radionuclide solubility, sorption and diffusion within the buffer.

2. Conceptual model and numerical implementation

2.1. Approach

Bentonite- (and broader, clay)-cement interactions constitute a complex system of coupled chemical-hydraulic-transport-mechanical processes (e.g. Takase, 2004). Compacted bentonite exhibits significant potential for chemical buffering of cement leachates due to processes such as montmorillonite surface protonation/de-protonation reactions, carbonate mineral dissolution, the dissolution of montmorillonite (and other silicates), and the precipitation of secondary minerals (e.g. zeolites and clay minerals). This complicated network of coupled

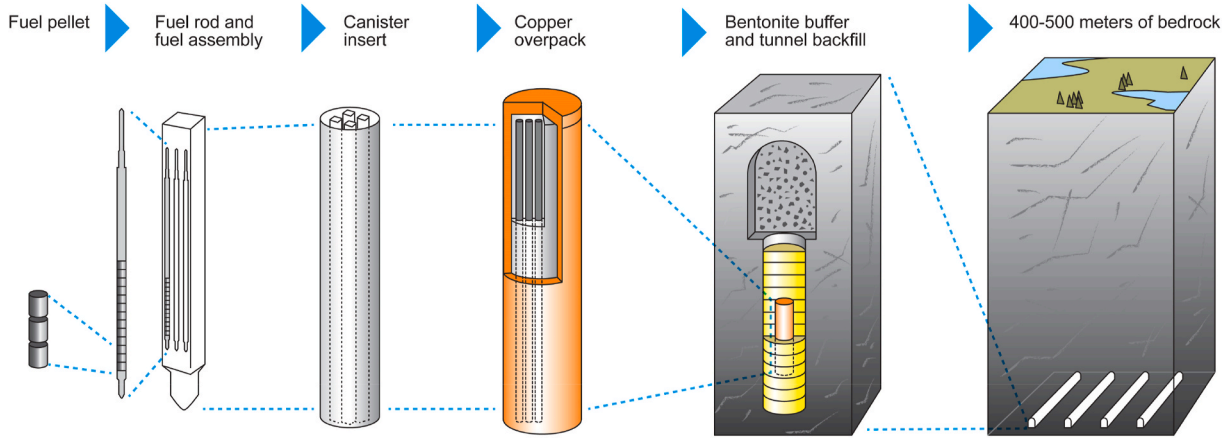

Fig. 1. Schematic of the POSIVA (KBS–V) concept for geological disposal of spent nuclear fuel (illustration courtesy of POSIVA Oy).

chemical reactions must be considered simultaneously with mass transport. Furthermore, porosity changes and their impact on solute transport need to be accounted for. In addition, mechanical effects (e.g. related to mineral dissolution and precipitation) can further complicate clay-cement interactions. Coupled reactive-transport models have proven to be a uniquely suited tool helping interpret experimental results on cement-clay interactions (e.g. Fernández et al., 2010 or Savage et al., 2011), and provide the best existing basis for extrapolations into the future over times-scales required by safety assessment.

Considering the problem at hand, the relevant process can be broadly conceptualised to include: (1) cement dissolution and generation of high-pH leachates, (2) transport of the leachates from the area of their production to the deposition hole *via* a network of interconnected fractures (associated with mixing, dilution and chemical interactions with the rock), and (3) interactions of the leachates with the bentonite buffer. However, due to computational burden that would result from a detailed and explicit representation of these processes over the large spatial and temporal scales involved, the geometry and some of the processes are represented in a simplified manner (as described in detail later).

Due to uncertainties related to interactions between cement leachates and bentonite, exact predictions of porewater evolution, especially over long times, are not feasible. However, the uncertainties can be bounded by a conservative choice of processes and parameter values. Here, by a "conservative" assumption is meant one that is expected to increase perturbation of the buffer porewater above what might realistically be predicted, and leads therefore to a more "pessimistic" outcome from the point of view of safety assessment. In this paper we set out by considering a *Base Case* defined by a combination of best-guess estimates (e.g. fracture aperture and flow rate through the fracture, kinetic rates of mineral reactions, and diffusivity of the buffer), and conservative assumptions where significant conceptual uncertainties and knowledge gaps arise (e.g. the composition of leachates contacting the buffer and porosity reduction due to mineral reactions in the buffer). The results of the *Base Case* are interpreted therefore as "conceivable bounding values".

In order to evaluate key *Base Case* model assumptions and simplifications, a set of auxiliary calculation cases is defined. These cases are designed to test the potential effects related to flow and transport processes (fracture aperture and flow rate, buffer diffusivity, and potential formation of a reduced porosity zone in the buffer due to mineral reactions), chemical reactions (dissolution of montmorillonite, and precipitation of secondary clay and zeolite minerals), and the composition of the inflowing cement leachate. Relative to the *Base Case*, some of the cases make further conservative assumptions (e.g. higher fracture aperture, higher flow, higher buffer diffusivity, slower montmorillonite dissolution rate, and no formation of secondary minerals). This is done to quantify the hypothetical maximum extent of buffer porewater perturbation, and to gain insight into the role of individual processes in the *Base Case* model. Other cases (regarding the composition of the fracture-inflowing fluid and the possible formation of a reduced-porosity zone in the buffer) explore probable effects (not included in the *Base Case*) that would tend to decrease the magnitude of buffer porewater perturbation. These cases are meant to serve as illustrative scenarios, the likelihood and extent of which are currently difficult or impossible to quantify rigorously.

Moreover, even in the event of complete absence of cement leachates in the vicinity of the deposition hole, the buffer will be contacted by the groundwater present in the host rock and interact with it. As a result, a change of the initial buffer pore water will occur over time. Although the evolution of the buffer porewater under "natural conditions" is not the focus of this paper (and the problem is not treated exhaustively), we consider it useful to perform such calculations (*Ref Saline* – see Section 2.4 for details) to provide a reference against which the *Base Case* results can be compared. The results of this case are meant to offer an additional (besides the initial state of the porewater) context within which the predicted magnitude of buffer porewater composition change can be discussed. It is emphasized however that this case is "stylised" and for the purpose of relative comparison only. Besides the *Base Case* and *Reference Case* calculations, a number of sensitivity cases are presented. These calculations serve to quantify selected model uncertainties.

Change of the buffer porewater is defined relative to the initial composition. For components, change is expressed as the ratio of the current (at the time considered) to initial concentrations, and presented in the log10(change) form, where null corresponds to no change – this ensures symmetry and additivity of results. For pH (log10 of proton activity), change is defined as the difference of the current and initial pH values.

2.2. Model geometry

For computational feasibility, model domain is restricted to the vicinity of the deposition hole as shown in Fig. 2. The fracture is idealised to intersect the buffer horizontally at mid-height (and is therefore perpendicular to the vertical deposition hole hosting the buffer). The fracture bounding planes are parallel and perfectly smooth, and the fracture extends a minimum of 1 m away from the external edge of the buffer. Water inflow occurs on one side of the fracture, and outflows on the opposite, as indicated in Fig. 2. The external boundary of the fracture is closed to flow and transport.

The vertical extent of the model is 2 m (1 m above and below the fracture plane). Note that a plane of symmetry running horizontally through the middle of the fracture allows the geometry to be reduced to a ½ for more efficient computation. The top and bottom sides of the buffer are closed to transport. The truncated geometry of the deposition hole along with the closed transport boundary conditions on the top and bottom faces of the buffer tend to increase the perturbation of the buffer porewater due to interactions with cement leachates, and are therefore conservative.

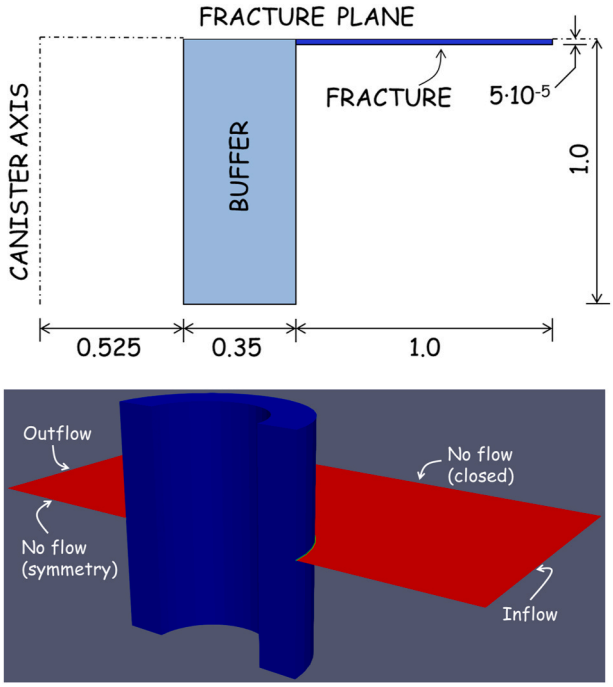

Fig. 2. Dimensions [m] of the model (top – a vertical cross-section of ¼ geometry, not to scale) and a vertical cross-section of the full model geometry indicating flow boundary conditions (bottom – buffer in blue, fracture in red) Note that the canister and rock are considered impervious to flow and transport, and not included. Fracture aperture corresponds to the *Base Case* value of 10^{-4} m. (For interpretation of the references to colour in this figure legend, the reader is referred to the Web version of this article.)

2.3. Buffer

Within the buffer, relevant processes for chemical porewater composition include: diffusive solute transport, mineral dissolution and precipitation reactions, other chemical reactions (e.g. cation exchange, surface and aqueous complexation), and porosity and diffusivity changes due to mineral reactions. Advective flow and solute transport in the buffer are represented, but due to low permeability ($5{\cdot}10^{-21}$ [m^2] – Pintado and Rautioaho, 2013) are negligible. The buffer is fully water-saturated at all times.

2.3.1. Initial composition and chemical reactions

The buffer material is MX-80 bentonite – a high grade Na-bentonite from Wyoming (POSIVA, 2012a). Buffer dry density and total porosity are 1557 [kg/m^3] and 0.43, respectively (based on Juvankoski, 2017). The mineral composition of the buffer is simplified to include gypsum, calcite, quartz, kaolinite, goethite and montmorillonite as primary reactive minerals (Table 1; Kiviranta et al., 2018) – remaining minerals are treated as inert. The Na-dominated Montmorillonite-BCNa from the Thermochimie thermodynamic database v.9b0 (www.thermochimie-tdb.com and Giffaut et al., 2014) is selected as it was found to be closest in composition to the data reported by Kiviranta et al. (2018). Additional reactions include cation exchange for Na, Ca, Mg and K (Table 2; Bradbury and Baeyens, 2003), and montmorillonite surface protonation (Table 2; Bradbury and Baeyens 1997). The cation exchange capacity (CEC) of the bentonite buffer (Table 2) is defined based on data in Kiviranta et al. (2018). The initial buffer porewater composition is calculated following a modified methodology of Bradbury and Baeyens (2003). Table 1 presents the initial porewater, mineral and cation exchanger compositions.

Exchange and complexation reactions are assumed to occur instantaneously (at equilibrium). Mineral reactions in reactive transport calculations are kinetic. The dissolution kinetic rate equation (Equation (1)) and its parameterization (Table 3) for quartz, kaolinite and montmorillonite are taken from Marty et al. (2015) with specific mineral surface areas presented in Table 2. Note that mineral precipitation rates are assumed to equal the dissolution rates. Porosity is assumed to be constant in time and mineral volume changes due to dissolution/precipitation reactions are not directly coupled to transport properties (e.g. diffusivity and permeability) – however, as discussed below, the potential impact of porosity changes on diffusivity is simplistically treated in selected sensitivity cases. Also, the concentration of surface protonation and cation exchanger sites scale with montmorillonite content (e.g. sorption capacity decreases as a result of montmorillonite dissolution). For gypsum, calcite and goethite the kinetic rate is adjusted to mimic local chemical equilibrium.

$$k = k_{25}^{nu} exp\left[\frac{-E_a^{nu}}{R}\left(\frac{1}{T}-\frac{1}{298.15}\right)\right] + k_{25}^{H} exp\left[\frac{-E_a^{H}}{R}\left(\frac{1}{T}-\frac{1}{298.15}\right)\right] a_H^{n_H} + k_{25}^{OH} exp\left[\frac{-E_a^{OH}}{R}\left(\frac{1}{T}-\frac{1}{298.15}\right)\right] a_{OH}^{n_{OH}} \quad (1)$$

However, it is known that laboratory-derived mineral dissolution rates are often several orders of magnitude higher than those found in nature (e.g. Lüttge et al., 2013; Marty et al., 2009; Velbel, 1990; White and Brantley, 2003; Zhu, 2005). This uncertainty is simplistically bounded by considering a sensitivity case (*Mnt Rate Low*), whereby the alkaline dissolution rate constant of montmorillonite ($2.9{\cdot}10^{-12}$ [mol/m^2/s]) is decreased 100 000 times (to $2.9{\cdot}10^{-17}$ [mol/m^2/s]).

Besides primary minerals initially present in the buffer, 33 secondary minerals are allowed to precipitate, if over-saturated. The minerals are selected based on a literature data review (Savage et al., 2002, 2007; Gaucher et al., 2004; Gaucher and Blanc, 2006; Pfingsten et al., 2006; Gaboreau et al., 2011) and are listed in Table 4.

Precipitation kinetics of many of these secondary minerals is poorly known (Savage et al., 2007), but the rates are usually expected to be faster than the rate of montmorillonite dissolution (Steefel and Lichtner, 1998). Therefore, unless indicated otherwise, the precipitation rates of the neo-formed minerals are adjusted to be in excess of the montmorillonite dissolution rate. In addition to that, an unlikely bounding case is considered (*No Sec Min*), whereby the precipitation of all secondary minerals shown in Table 4 is completely supressed.

2.3.2. Solute transport

Due to low buffer permeability ($5{\cdot}10^{-21}$ [m^2] – Pintado and Rautioaho, 2013), water flow and advective solute transport in the buffer are negligible. Therefore, aqueous diffusion is the main solute transport mechanism in the buffer. Diffusion in compacted clays is known to be complicated by electrostatic interactions due to the presence of charged

Table 1
Initial porewater, mineral and exchanger compositions of the buffer. [(1)]Represented by Montmorillonite-BCNa as defined in the Thermochimie thermodynamic database v.9b0 (www.thermochimie-tdb.com). [(2)]Traces of kaolinite assumed to be present.

Parameter	Value
pH	8.00
Total dissolved	[mol/L]
Al	$1.86{\cdot}10^{-8}$
C(IV)	$3.36{\cdot}10^{-4}$
Ca	$1.47{\cdot}10^{-2}$
Cl	$7.42{\cdot}10^{-2}$
K	$3.38{\cdot}10^{-4}$
Mg	$3.69{\cdot}10^{-3}$
Na	$1.13{\cdot}10^{-1}$
Fe	$9.03{\cdot}10^{-7}$
S(VI)	$3.74{\cdot}10^{-2}$
Si	$1.84{\cdot}10^{-4}$
Minerals	[wt%]
[(1)]Montmorillonite	82.6
[(2)]Kaolinite	0.1
Quartz	3.8
Calcite	0.83
Goethite	0.23
Gypsum	1.07
Exchanger	[CEC fraction]
NaX	0.74
CaX_2	0.18
MgX_2	0.07
KX	0.01

Table 2
Specific mineral surface areas, cation exchange and surface protonation reactions, and CEC and surface site capacity values used in this study. [(1)]Marty et al. (2015), [(2)]Huertas et al. (1998), [(3)]Bradbury and Baeyens (2003), [(4)]Kiviranta et al. (2018), [(5)]Bradbury and Baeyens (1997).

Mineral	Specific surface area [m^2/g]
[(1)]Montmorillonite	8.5
[(2)]Kaolinite	8.2
[(1)]Quartz	0.03
[(3)]Cation exchange reaction	Selectivity coefficient
$NaX + K^+ = KX + Na^+$	4
$2NaX + Mg^{2+} = MgX_2 + 2Na^+$	2.2
$2NaX + Ca^{2+} = CaX_2 + 2Na^+$	2.6
[(4)]Cation exchanger capacity	[eq/kg_{buffer}]
CEC	0.93
[(5)]Surface reaction	logK
$>S_sOH + H^+ = >S_sOH_2^+$	4.5
$>S_sOH = >S_sO^- + H^+$	−7.9
$>S_{w1}OH + H^+ = >S_{w1}OH_2^+$	4.5
$>S_{w1}OH = >S_{w1}O^- + H^+$	−7.9
$>S_{w2}OH + H^+ = >S_{w2}OH_2^+$	6.0
$>S_{w2}OH = >S_{w2}O^- + H^+$	−10.5
[(5)]Site type	[mol/$kg_{montmorillonite}$]
$>S_sOH$	$2{\cdot}10^{-3}$
$>S_{w1}OH$	$4{\cdot}10^{-2}$
$>S_{w2}OH$	$4{\cdot}10^{-2}$

Table 3
Kinetic dissolution rate model parameters (from Marty et al., 2015). Kinetic constants (k) are expressed in [mol/m^2/s] and the activation energy (E_a) in [kJ/mol].

Mineral	k_{25}^{nu}	E_a^{nu}	k_{25}^{H+}	E_a^{H+}	n^{H+}	k_{25}^{OH-}	E_a^{OH-}	n^{OH-}
Montmorillonite	$9.3\cdot10^{-15}$	63	$5.3\cdot10^{-11}$	54	0.69	$2.9\cdot10^{-12}$	61	0.34
Kaolinite	$1.1\cdot10^{-14}$	38	$7.5\cdot10^{-12}$	43	0.51	$2.5\cdot10^{-11}$	46	0.58
Quartz	$6.4\cdot10^{-14}$	77				$1.9\cdot10^{-10}$	80	0.34

Table 4
List of secondary minerals (as defined in the Thermochimie thermodynamic database v.9b0 – www.thermochimie-tdb.com) allowed to form, if oversaturated, due to interactions between the bentonite buffer and the cementitious leachates.

Secondary Minerals		
Chalcedony	Celadonite-Fe	Tobermorite-14A
Nontronite-Ca	Celadonite-Mg	Gyrolite
Nontronite-Na	Illite-Al	Stratlingite
Nontronite-Mg	Illite-FeIII	Katoite
Nontronite-K	Illite-Mg	Dolomite
Mordenite	Beidellite-Ca	Siderite
Clinoptilolite_Ca	Beidellite-K	Brucite
Clinoptilolite_K	Beidellite-Mg	Hydrotalcite
Clinoptilolite_Na	Beidellite-Na	Ettringite
Saponite-FeCa	Albite-low	Ettringite-Fe
Saponite-FeK	Tobermorite-11A	Gibbsite

montmorillonite surfaces, resulting in partial ion exclusion from the pore space. For computational feasibility, a simplified model is used, whereby diffusion takes place within a single (total) porosity of the bentonite, while all diffusing species have the same constant effective diffusion coefficient of $4.4\cdot10^{-11}$ [m^2/s] (*Base Case* value estimated based on an empirical relationship reported in Wersin et al., 2014). The uncertainty related to using such simplified representation of diffusion is difficult to quantify in a general case. However, based on previous experience and best judgement, two cases are proposed to bracket this uncertainty: (a) D_e three times higher than *Base Case* value (*High De*, $1.3\cdot10^{-10}$ [m^2/s]), (a) D_e three times lower than *Base Case* value (*Low De*, $1.5\cdot10^{-11}$ [m^2/s]). Incidentally, the higher end of the diffusion coefficient corresponds to an approximately factor 3 increase in diffusivity related to temperature increase from 25 °C to 70 °C (Wersin et al., 2014).

Mineral reactions associated with cement leachates interactions with clays are known to induce porosity changes (e.g. Read et al., 2001; De Windt et al., 2008; Gaboreau et al., 2011). Typically observed is the formation of a narrow zone of reduced porosity, where water flow and solute transport are decreased. However, the extent of porosity reduction and, especially, its impact on flow and transport properties of the clay are currently difficult to quantify. Therefore, unless otherwise indicated, the calculations presented conservatively ignore porosity reduction and its potential effect on water flow and solute transport. Additionally, two sensitivity cases are defined, whereby porosity is arbitrarily reduced within a 1 cm by 1 cm thick zone of the buffer along the fracture/bentonite contact perimeter. The porosity in these cases is constant in time and space throughout the calculation and reduced to 10% (*Skin Poro 10%*) and 1% (*Skin Poro 1%*), respectively (compare to the *Base Case* value of 43%). In a simplistic manner, these cases are meant to provide an illustration of the potential effects related to porosity reduction and its impact on solute diffusion into the buffer. Note that a linear dependence of the effective diffusion coefficient on porosity is assumed, and that the effect of porosity reduction on permeability is ignored.

2.4. Fracture and the rock

The rocks of Olkiluoto consist of high-grade metamorphic rocks (migmatised gneisses) and igneous rocks (pegmatitic granites and diabase dykes). The bedrock has been affected by deformations and is fractured, while the properties of the fractures have been hydrothermally altered. Groundwater flow concentrates in hydraulically active deformation zones (hydrogeological zones) and in individual fractures. The hydrogeological zones and the fractures are collectively termed water-conducting features, and form a connected network of paths for solute transport. A general trend is observed whereby the frequency of transmissive fractures, and the transmissivity of both fractures and the hydrogeological zones decrease with depth. Details on the geology and hydrogeology of the site can be found in POSIVA (2012c).

2.4.1. Geometry, flow, transport and chemical reactions

At the prospective repository depth, Discrete Fracture Network (DFN) models have been used by POSIVA to describe in detail groundwater flow in the vicinity of deposition tunnels and deposition holes (refer to POSIVA 2012c and references therein). The DFN models have been developed based on a detailed statistical analysis of fracture mapping data from the drillholes, outcrops and rock walls at ONKALO®. Hydrogeological properties of the stochastically modelled fractures are derived from pumping tests. The hydro-DFN model is appropriate to describe groundwater flow at the detailed scale in the vicinity of a deposition hole (POSIVA, 2012c). Based on this model, unless otherwise indicated, calculations consider a fracture aperture of 10^{-4} m and a constant flow of 10^{-3} [$m^3_{water}/m_{fracture\ length}$/y], which corresponds to the 50th percentile of measured values (POSIVA, 2012d). This combination of fracture aperture and flow yields an average linear flow velocity of 10 [m/y]. The *Base Case* flow field in the fracture is presented in Fig. 3. In addition, two sensitivity cases are defined. In the *Frac High* case both the aperture and volumetric flow rate are increased ten times (yielding an average linear flow rate of 10 [m/y], as in the *Base Case*) – corresponding to the 90th percentile of the reported values (POSIVA, 2012d). In the *Frac Low* case the aperture is maintained at 0.1 mm, while the volumetric flow rate is reduced 10 times (yielding an average flow velocity of 1 [m/y]) – corresponding to the 10th percentile of the reported flow values (POSIVA, 2012d).

The fracture is idealised to be bounded by parallel, perfectly smooth planes, with a spatial extent limited to ca. 1 m away from the external

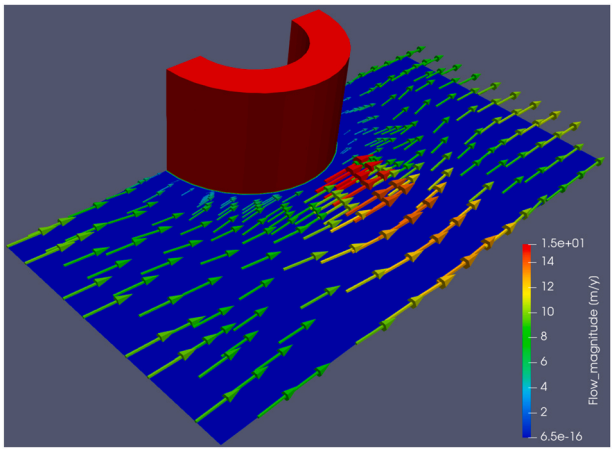

Fig. 3. *Base Case* steady state flow field in the fracture (blue) around the buffer (red). Flow magnitude scale [m/y] refers to arrow colour. (For interpretation of the references to colour in this figure legend, the reader is referred to the Web version of this article.)

edge of the buffer. The fracture is assumed to have unity porosity and be completely water-filled. In the fracture, solute transport is due to a combination of advection (with no hydrodynamic dispersion) and diffusion. However, advective solute transport dominates, especially further away from the buffer.

The fracture is assumed to contain no primary minerals, however, secondary minerals (as listed in Table 4) are permitted to precipitate, if over-saturated. The precipitation of secondary minerals is assumed to have no effect on the flow and solute transport properties in the fracture (i.e. no porosity feedback on flow and transport).

2.4.2. Composition of inflowing solution

Cements will be used during the construction and operation of the repository, mainly, to limit groundwater inflow through fractures, for stabilisation of the rock, and as plugs in the engineered barrier system (POSIVA, 2012b). In ONKALO®, standard cement has been used above the HZ20 fracture zone which is located approximately at a depth of 300 m. Below this feature, low-pH grout has been systematically used, except for rock bolt grouting. No cementitious materials are allowed in the deposition hole (POSIVA, 2012b). Presently, limited amounts of cementitious materials are, however, used in the deposition tunnels, such as in the end plug, rock bolts and for grouting of fractures. To avoid significant disturbance of natural groundwater pH conditions, low-pH cementitious materials producing alkaline leachates of pH < 11 or silica sol (colloidal silica) are utilised near the disposal depth (POSIVA, 2012b).

As follows from the restricted extent of the model geometry described earlier, the degradation of these cements and the transport of the resulting leachates in the repository's far field are not explicitly represented in the model. However, these processes are taken into account implicitly through the definition of transport boundary conditions on the fracture inflow as discussed below.

Soler (2010, 2011a, 2012) and Soler et al. (2011) performed reactive transport calculations to investigate the possible formation of a high-pH plume at the cement grout-rock interface in ONKALO®. The results suggest that the pH of the leachate near the grout will decrease rapidly as a result of mineral precipitation and porosity reduction in the grout, and mixing and dilution due to flowing groundwater. For standard cement, leachate pH at the cement/groundwater interface was predicted to decrease rapidly from the initial value of about 12.5 to below 11.5 within the first year of leaching. Furthermore, the model predicted a pH decrease to below 9 within a few tens of years at a point located 2 m downstream from the interface (Soler, 2010). These modelling results are corroborated by field observations in ONKALO®; for example, borehole monitoring data from sections grouted using standard cement show a rapid pH decrease from above 12 to below 10 within approximately 2 years (Soler, 2010).

Koskinen (2013) extrapolated the model results of Soler (2011) to mimic the expected long-term general cement degradation evolution for both standard- and low-pH-cements. For the standard cement, the pH of the leachate at the cement/groundwater interface was conservatively estimated to decrease below pH 10 within 10 000 years.

Based on laboratory experiments, POSIVA defined three discrete cement leachate compositions representing distinct stages of progressive degradation of standard cement (Table 5), which were used in previous modelling studies (e.g. Lehikoinen, 2009; Montori et al., 2008).

From the above discussion, for the *Base Case* calculation, we conservatively select the leachate composition corresponding to pH 11.60 as a constant transport boundary condition on the fracture inflow during a period of 10 000 years. Beyond that period, it is considered that a combination of pH decrease at the cement/groundwater interface and on transport by the groundwater would reduce leachate pH near the deposition hole to values comparable with those of the groundwater. For comparison, a leachate composition corresponding to pH 9.70 is also studied as a sensitivity case (case *pH 9.7*).

In addition, we define a reference case (*Ref Saline*), whereby the inflowing solution has the composition of the Saline groundwater (Table 6). It is reminded that this case serves for relative comparison purposes only, and is not intended to represent a specific future hydrological and climate evolution scenario. During leachate transport from the area of their production to the deposition hole (possibly tens to hundreds of metres), mixing with the groundwater will occur and lead to secondary mineral precipitation. Rigorous modelling of such processes is beyond the scope of this study. However, we consider three additional illustrative cases to simplistically demonstrate the effects associated with such mixing, dilution and precipitation of secondary minerals. In these cases the boundary transport solution is defined by mixing the pH 11.6 leachate with progressive amounts of the saline groundwater (Table 6): *10% Saline* (90% leachate and 10% saline groundwater), *50% Saline* (50% leachate and 50% saline groundwater), and *90% Saline* (10% leachate and 90% saline groundwater).

Mixing calculations were performed using the PHREEQC version 3 (Parkhurst and Appelo, 2013) geochemical simulator at 25 [°C] with the Thermochimie thermodynamic data base v.9b0 (https://www.thermochimie-tdb.com/) and the Lawrence Livermore National Laboratory (LLNL) parameterization of the extended Debye-Hückel aqueous activity model (Giffaut et al., 2014). During the calculations, minerals shown in Table 4 were allowed to precipitate if over-saturated.

The initial solution composition in the fracture corresponds to the transport boundary composition at the start of the calculation.

2.4.3. Rock

To facilitate calculations, the rock is assumed to be impervious to groundwater flow and solute transport. Scoping calculations performed using a simpler cylindrical geometry (not shown) indicate that due to its low diffusivity and permeability, the influence of the rock matrix is negligible compared to the effect of the fracture. Furthermore, matrix diffusion and potential chemical reactions of the cement leachates with rock minerals (e.g. pH buffering reactions involving Al-silicates) are ignored. Such processes would tend to neutralise the leachate's elevated pH and shift its composition towards that of the groundwater.

Table 5
Chemical composition of cement leachates (from Montori et al., 2008).

Total [mol/L]	pH 12.17	pH 11.60	pH 9.70
Al	10^{-6}	10^{-6}	10^{-6}
C(IV)	10^{-6}	10^{-6}	10^{-6}
Ca	0.12	0.11	0.10
Cl	0.42	0.42	0.41
K	$6{\cdot}10^{-4}$	$6{\cdot}10^{-4}$	$6{\cdot}10^{-4}$
Mg	10^{-6}	$4{\cdot}10^{-6}$	$2{\cdot}10^{-3}$
Na	0.21	0.21	0.205
S(VI)	$2.3{\cdot}10^{-5}$	$4{\cdot}10^{-5}$	$8{\cdot}10^{-5}$
Si	$5{\cdot}10^{-6}$	$2{\cdot}10^{-5}$	$7{\cdot}10^{-5}$

Table 6
Composition of the transport boundary solution for cases: *Ref Saline*, *10% Saline, 10% Saline and 10% Saline.*

	Ref Saline	90% saline	50% saline	10% saline
pH	7.28	8.93	10.89	11.57
Total component [mol/L]				
Al	$3.9{\cdot}10^{-9}$	$3.7{\cdot}10^{-16}$	$4.3{\cdot}10^{-18}$	10^{-10}
C(IV)	$6.6{\cdot}10^{-4}$	$1.9{\cdot}10^{-5}$	$6.9{\cdot}10^{-6}$	$6.7{\cdot}10^{-6}$
Ca	$3.3{\cdot}10^{-2}$	$4.0{\cdot}10^{-2}$	$7.1{\cdot}10^{-1}$	10^{-1}
Cl	$1.9{\cdot}10^{-1}$	$2.1{\cdot}10^{-1}$	$3.0{\cdot}10^{-1}$	$4.0{\cdot}10^{-1}$
Fe	$9.5{\cdot}10^{-6}$	$9.5{\cdot}10^{-8}$	$3.7{\cdot}10^{-10}$	$6.6{\cdot}10^{-6}$
K	$2.8{\cdot}10^{-4}$	$3.2{\cdot}10^{-4}$	$4.4{\cdot}10^{-4}$	$5.7{\cdot}10^{-4}$
Mg	$2.6{\cdot}10^{-3}$	$2.2{\cdot}10^{-3}$	$9.7{\cdot}10^{-5}$	$6.6{\cdot}10^{-6}$
Na	$1.2{\cdot}10^{-1}$	$1.3{\cdot}10^{-1}$	$1.6{\cdot}10^{-1}$	$2.0{\cdot}10^{-1}$
S(VI)	$2.1{\cdot}10^{-4}$	$2.0{\cdot}10^{-4}$	$1.3{\cdot}10^{-4}$	$5.8{\cdot}10^{-5}$
Si	$1.8{\cdot}10^{-4}$	$2.2{\cdot}10^{-5}$	$5.2{\cdot}10^{-6}$	$4.0{\cdot}10^{-6}$

2.5. Summary of calculation cases

All calculation cases considered in this study are summarised in Table 7. The rationale for selecting these cases and their specific parameterization was discussed earlier. In summary, relative to the *Base Case*:

- The *Ref Saline* case assumes the saline groundwater as the fracture transport boundary and initial solution (absence of cement leachates).
- The *Frac High* case assumes ten times higher aperture and volumetric water flow (yielding average flow velocity of 10 [m/y], as in the *Base Case*), while the *Frac Low* case assumes the same aperture as in the *Base Case*, but ten times lower volumetric flow rate (yielding an average flow velocity of 1 [m/y]).
- *Skin Poro 10%* and *Skin Poro 1%* cases assume the presence of a small (approximately 1 cm by 1 cm) area of the buffer characterised by reduced porosity (10% and 1%, respectively) at the buffer contact with the fracture.
- *De High* and *De Low* cases assume 3 times higher and 3 times lower effective diffusion coefficients for the buffer, respectively.
- *Mnt Rate* Low case assumes that the maximum dissolution rate of montmorillonite is 100 000 times lower.
- *No Sec Min* case assumes complete suppression of secondary zeolite and clay mineral precipitation.
- *pH 9.7* case assumes the pH 9.7 cement leachate (Table 5) as the fracture transport boundary and initial solution.
- *10% saline, 50% saline* and *90% saline* cases consider a mixture of the pH 11.6 cement leachate (Table 6) with 10%, 50% and 90% of the saline groundwater, respectively, as the fracture transport boundary and initial solution.

2.6. Numerical implementation

Calculations are performed using the PFLOTRAN code. Details regarding the technical capabilities of the code can be found in Hammond et al. (2012, 2014 and 2019), or at www.pflotran.org. PFLOTRAN uses the finite volume method to solve a system of generally nonlinear partial differential equations describing reactive flow and reactive transport in porous materials. The spatial discretization is variable in space (Fig. 4). Cells located near the buffer contact with the fracture are of 1 cm size and increase gradually further away from the contact. The Base Case grid, composed of about 15 500 cells, was optimised through a series of scoping calculations (not presented) to provide fine refinement in the fracture/buffer intersection area, while allowing for satisfactory numerical convergence and acceptable solution times. PFLOTRAN uses an automatic step adjustment algorithm that, based on the user-defined tolerance criteria, aims to increase the solver time step towards a user-defined maximum value. In the present calculations, the relative update of the solution (STOL) with a value of 10^{-5} was used as the convergence criterion. This value was optimised by running test calculations and comparing the results against more stringent STOL values. The maximum time step allowed was defined at 0.1 year. Scoping calculations showed that further decrease in the maximum time size had no observable effect on the results.

Calculations were performed on the University of Bern High Performance Computing cluster computer Ubelix (https://ubelix.unibe.ch/). A single calculation typically utilised 80 processors in parallel and, depending on solution convergence, took up to about 20 h to complete.

Reactive transport calculations were performed at 25 °C using the Thermochimie thermodynamic data base v.9b0 (https://www.thermochimie-tdb.com/) utilising the Lawrence Livermore National Laboratory (LLNL) parameterization of the extended Debye-Hückel aqueous activity model (Giffaut et al., 2014). The primary species include (note that the sulfate-sulphide redox couple is decoupled): H^+, $O_2(aq)$, Na^+, Mg^{++}, Ca^{++}, Sr^{++}, K^+, Fe^{++}, Al^{+++}, $H_4(SiO_4)$, Cl^-, CO_3^{--}, SO_4^{--} and HS^-. As secondary, the following species are considered: OH^-, H_2S, KSO_4^-, $CaSO_4$, $CaCO_3$, $CaHCO_3^+$, $CaCl^+$, $CaCl_2$, $CaOH^+$, $SrSO_4$, $SrCl^+$, $SrHCO_3^+$, CO_2, HCO_3^-, Fe^{+++}, $FeCO_3OH$, $Fe(OH)_2$, $Fe(OH)_2^+$, $Fe(OH)_3$, $Fe(OH)_3^-$, $Fe(OH)_4^-$, $Fe(OH)_4^-$, $FeOH^+$, $FeOH^{++}$, $FeCO_3$, $FeCl^+$, $FeCl^{++}$, $FeCl_2$, $FeCl_2^+$,

Table 7
Summary of calculation cases with main differences relative to the *Base Case*. *a* – fracture aperture, *v* – average linear water flow velocity in the fracture, *NA* – not applicable. See further explanations in text.

	Flow & transport			Mineral reactions		Fracture inflow transport boundary
	Fracture aperture & flow	Skin porosity [%]	Buffer De [m^2/s]	k Mnt OH^- [$mol/m^2/s$]	Second min rate	
Ref Saline	$a = 10^{-4}$ m $v = 10$ m/y	NA	$4.4{\cdot}10^{-11}$	$2.9{\cdot}10^{-12}$	In excess of Mnt diss	Saline GW
Base Case	**$a = 10^{-4}$ m** **$v = 10$ m/y**	**NA**	**$4.4{\cdot}10^{-11}$**	**$2.9{\cdot}10^{-12}$**	**In excess of Mnt diss**	**pH 11.6**
Frac High	$a = 10^{-3}$ m $v = 10$ m/y	NA	$4.4{\cdot}10^{-11}$	$2.9{\cdot}10^{-12}$	In excess of Mnt diss	pH 11.6
Frac Low	$a = 10^{-4}$ m $v = 1$ m/y	NA	$4.4{\cdot}10^{-11}$	$2.9{\cdot}10^{-12}$	In excess of Mnt diss	pH 11.6
Skin poro 10%	$a = 10^{-4}$ m $v = 10$ m/y	10	$4.4{\cdot}10^{-11}$	$2.9{\cdot}10^{-12}$	In excess of Mnt diss	pH 11.6
Skin poro 1%	$a = 10^{-4}$ m $v = 10$ m/y	1	$4.4{\cdot}10^{-11}$	$2.9{\cdot}10^{-12}$	In excess of Mnt diss	pH 11.6
De High	$a = 10^{-4}$ m $v = 10$ m/y	NA	$1.3{\cdot}10^{-10}$	$2.9{\cdot}10^{-12}$	In excess of Mnt diss	pH 11.6
De Low	$a = 10^{-4}$ m $v = 10$ m/y	NA	$1.5{\cdot}10^{-11}$	$2.9{\cdot}10^{-12}$	In excess of Mnt diss	pH 11.6
Mnt Rate Low	$a = 10^{-4}$ m $v = 10$ m/y	NA	$4.4{\cdot}10^{-11}$	$2.9{\cdot}10^{-17}$	In excess of Mnt diss	pH 11.6
No Sec Min	$a = 10^{-4}$ m $v = 10$ m/y	NA	$4.4{\cdot}10^{-11}$	$2.9{\cdot}10^{-12}$	Null	pH 11.6
pH 9.7	$a = 10^{-4}$ m $v = 10$ m/y	NA	$4.4{\cdot}10^{-11}$	$2.9{\cdot}10^{-12}$	In excess of Mnt diss	pH 9.7
10% saline	$a = 10^{-4}$ m $v = 10$ m/y	NA	$4.4{\cdot}10^{-11}$	$2.9{\cdot}10^{-12}$	In excess of Mnt diss	10% saline
50% saline	$a = 10^{-4}$ m $v = 10$ m/y	NA	$4.4{\cdot}10^{-11}$	$2.9{\cdot}10^{-12}$	In excess of Mnt diss	50% saline
90% saline	$a = 10^{-4}$ m $v = 10$ m/y	NA	$4.4{\cdot}10^{-11}$	$2.9{\cdot}10^{-12}$	In excess of Mnt diss	90% saline

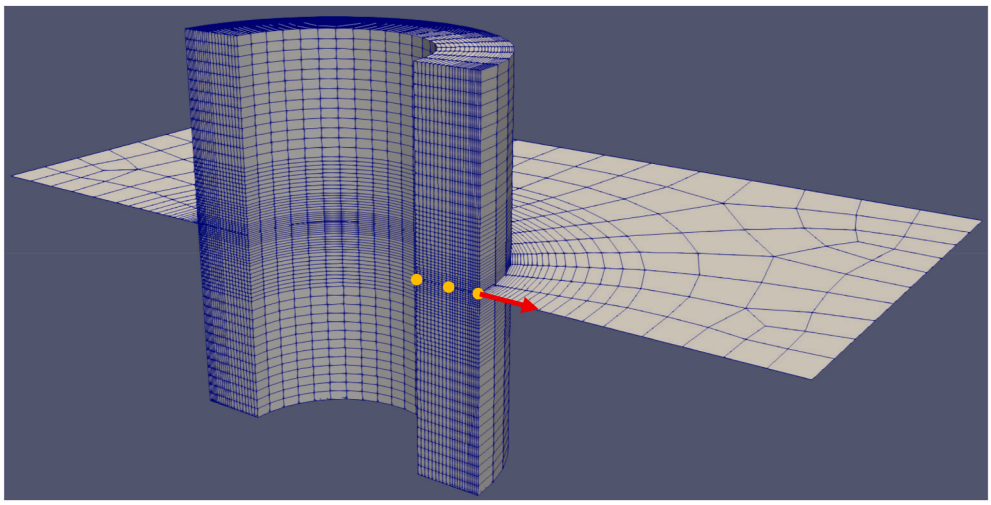

Fig. 4. Finite volume computational grid (half geometry) used in the calculations. Orange points schematically indicate the locations of observation points (general water flow is right to left). Indicated schematically as a red arrow is the position and orientation of a profile used to present mineral data. (For interpretation of the references to colour in this figure legend, the reader is referred to the Web version of this article.)

$FeCl_4^-$, $H_2(aq)$, $FeCl_3^-$, $FeCl_3$, $FeHS^+$, $FeSO_4$, $FeSO_4^+$, $AlOH^{++}$, $Al(OH)_2^+$, $Al(OH)_3$, $Al(OH)_4^-$, $MgCO_3$, $MgCl^+$, $MgHCO_3^+$, $MgOH^+$, $MgSO_4$, NaCl, $NaHCO_3$ and $NaSO4^-$.

3. Results and discussion

Results are presented as time-series at three observation points located: (a) in the buffer directly adjacent to the fracture, (b) at the buffer's mid-thickness, (c) in the buffer directly adjacent to the canister. Fig. 4 indicates schematically the location of the observation points within the model geometry. In addition, mineral volume fractions are presented along a profile running in the middle of the fracture from the buffer/fracture interface in the direction against leachates flow (Fig. 4). Results for water chemistry are shown as log10(change) of component concentration and pH difference between the current and initial values. In the discussion, component concentration change is also used. Results for cation exchange and surface sites reactions are shown as concentration (mol/m^3_{bulk}).

3.1. Base and reference cases

Time series of total component log10(change) and pH difference at the three observation points in the buffer over 10 000 years for the *Base Case* are shown in Fig. 5. The direction of change in the buffer porewater composition is largely defined by concentration gradients between the buffer porewater and the leachate. In addition, changes of dissolved solutes are affected by chemical reactions within the buffer. For example, dissolved sulfate from the buffer porewater diffuses into the fracture, while dissolved Ca diffuses in the opposite direction. Under gypsum equilibrium in the buffer, the decrease in dissolved sulfate is consistent with the increase in dissolved Ca. Similarly, dissolved carbonate diffuses from the buffer into the fracture, while dissolved Ca diffuses in the opposite direction. The resulting increase in dissolved Ca and pH, and decrease in dissolved carbonate are consistent with calcite equilibrium. The magnitude of the porewater perturbation can be seen to generally increase in time, albeit at a decreasing rate. For certain components, notably for hydrogen ion (pH), the perturbation tends to decrease at later times due to buffering by mineral dissolution/precipitation and surface protonation/de-protonation reactions. This is particularly the case at the observation point located near the fracture, where concentration changes are strongest.

Maximum buffer perturbation values during 10 000 years calculated at the three observation points for the *Base Case* and the *Saline Reference* case are shown in Table 8. The greatest perturbation is predicted for chloride, log10(change) of 0.56 (or an increase by a factor of 3.6 relative to initial concentration).

As discussed earlier, due to limited vertical extent of the model geometry and closed top and bottom transport boundaries, the model tends to over-estimate the buffer porewater perturbation. This affects especially non-reacting components, such as chloride. Despite this, at 10 000 years, chloride concentration in the buffer is predicted to be lower than the value of the leachate, which indicates that diffusive equilibration has not yet been completed – the log10(change) at complete diffusive equilibration would correspond to 0.76 or a change by factor of 5.7. This slow equilibration is due to limited mass transfer from the 0.1 mm thick fracture into the buffer, and limited buffer diffusivity.

Relative to the initial value, the concentration of dissolved carbonate in the buffer porewater is calculated to decrease by a maximum factor of ca. 2.5 near the canister (log10(change) of −0.7) or about twice that value near the fracture. The decrease is mainly due to out-diffusion of dissolved carbonate from the buffer porewater (initial concentration of $3.36{\cdot}10^{-4}$ [mol/L]) towards the fracture (leachate concentration of 10^{-6} [mol/L]).

The ca. factor 2 decrease in dissolved sulfate concentration at 10 000 years relative to the initial value (log10(change) of −0.29) is in agreement with gypsum equilibrium. Gypsum in the buffer is predicted to dissolve in the inner parts, and precipitate near the buffer's contact with the fracture (where dissolved calcium is supplied by the leachate). However, even at 10 000 years the extent of gypsum dissolution is insignificant (not shown). At the theoretical end point of complete gypsum dissolution, the associated sulfate concentration decrease would be almost 1000-fold.

The predicted moderate changes in the concentrations of carbonate and sulfate indicate that in combination with limited mass exchange between the buffer porewater and the cement leachate, chemical reactions in the buffer play an important role in resisting the porewater perturbation caused by interactions with the leachate. This is even more pronounced for silicon and aluminium – components involved in multiple secondary mineral precipitation reactions – the concentrations of which show little or negligible extent of disturbance.

The concentrations of major cations in solution, Ca^{2+}, Mg^{2+}, Na^+ and K^+, are predicted to increase by a factor of ca. 1.5 to 3. Except Mg^{2+}, this increase is largely due to diffusive supply of these components from the leachate in the fracture. The concentration of dissolved Mg^{2+} increases above the initial concentration in the buffer porewater, despite the leachate having lower Mg concentration than the buffer porewater,

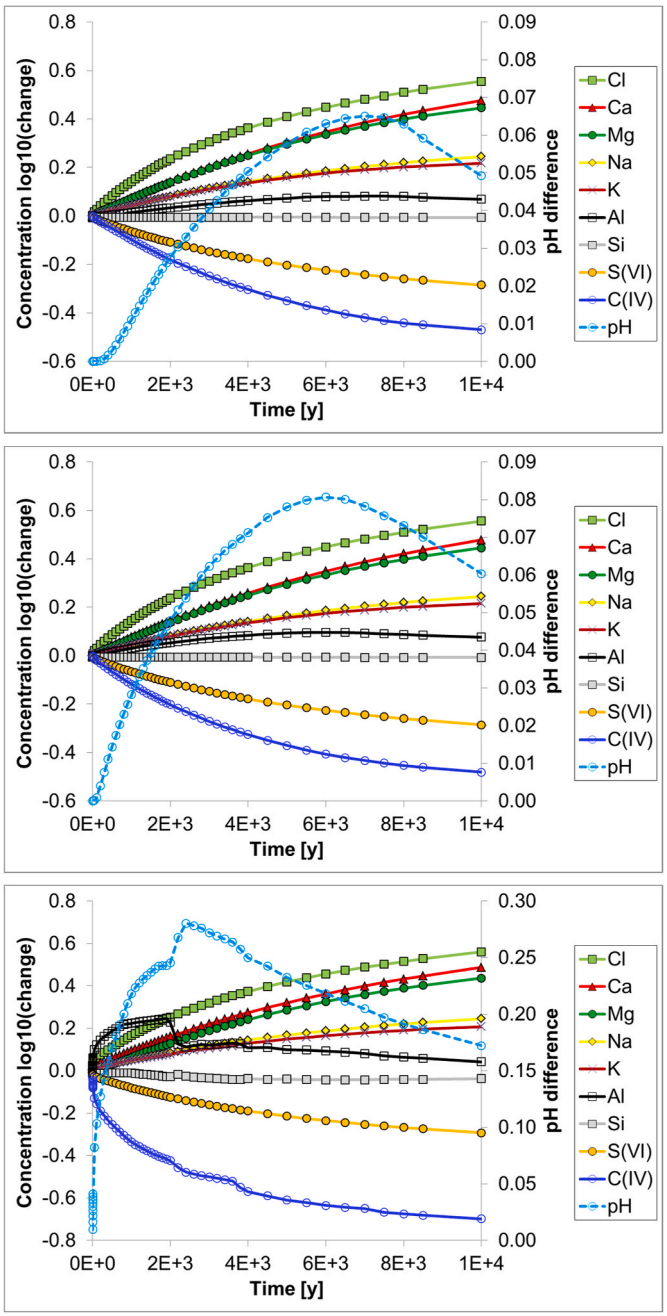

Fig. 5. *Base Case* concentration log10(change) of total components and pH difference at three observation points (top – near canister, middle – middle buffer, bottom – near fracture; see Fig. 4) during 10 000 years. The initial composition of the buffer porewater is shown in Table 1.

which is caused by Ca^{2+} from the leachate replacing Mg^{2+} on the cation exchanger (Fig. 6).

Over 10 000 years, the predicted pH changes are below 0.1 pH unit in most of the buffer volume. Only within a restricted zone of the buffer directly adjacent to the fracture local maximum pH change is predicted to be in the order of 0.3 pH. Notably, peak pH changes occur at a certain time (6–8 thousand years within most of the affected buffer volume, or 2 to 3 thousand years in a smaller zone directly at the fracture's contact), following which, the disturbance tends to decrease gradually, due to continued precipitation of secondary minerals and diffusion.

As mentioned in the introduction, to evaluate the potential effects of cement leachates on buffer porewater composition POSIVA has employed a conservative approach, whereby a pH value of 10 is imposed

Table 8
Comparison of maximum log10(change) of total components and maximum pH difference at the three observation points during 10 000 years for the *Saline Ref* and *Base Case*. Refer to Table 7 for additional explanations.

Total component	Saline Ref			Base Case		
	near can	mid buff	near frac	near can	mid buff	near frac
	Maximum log10(change) during 10 000 years					
Cl	0.26	0.26	0.27	0.56	0.56	0.56
Ca	0.17	0.17	0.17	0.48	0.48	0.49
Mg	0.16	0.16	0.16	0.45	0.44	0.44
Na	0.09	0.09	0.09	0.25	0.25	0.25
K	0.09	0.09	0.09	0.22	0.22	0.21
Al	−0.01	−0.01	−0.03	0.08	0.10	0.25
Si	−0.01	−0.01	−0.01	−0.01	−0.01	−0.04
S(VI)	−0.13	−0.13	−0.14	−0.28	−0.29	−0.29
C(IV)	−0.17	−0.17	−0.15	−0.47	−0.48	−0.70
	Maximum difference during 10 000 years					
pH	−0.01	−0.02	−0.03	0.07	0.08	0.28

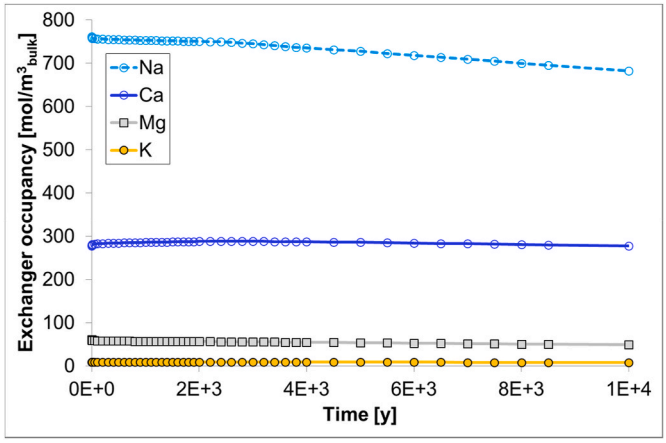

Fig. 6. *Base Case* composition of cation exchanger at the observation point in the buffer near the fracture (see Fig. 4).

onto the initial buffer porewater leading to a pH change of about 2 units. The present calculations indicate that, due to strong buffering properties, even considering a leachate pH of 11.6, the buffer porewater pH change should be expected to be much lower, below 0.1 pH unit.

A comparison with the reference case (*Ref Saline* – Table 8) can be used to put the calculated *Base Case* buffer porewater perturbation in further context. Even in complete absence of any cement leachates, a perturbation of the initial buffer porewater is expected due to interactions with the surrounding groundwater. For example, during the 10 000 years evaluation period, the maximum change predicted for dissolved Ca, Mg and carbonate is by a factor of ca. 1.5 (Table 8). Relative to the reference case, the *Base Case* calculation predicts a maximum perturbation of the buffer porewater that would be greater than this "natural" perturbation by a factor of 2 or less in most of the buffer volume.

In line with the limited extent of porewater perturbation, the initial composition of the *Base Case* cation exchanger is predicted to change little during 10 000 years, including at the contact with the fracture (Fig. 6) – note a decrease in the CEC (ca 10%) due to montmorillonite dissolution.

Fig. 7 shows the contribution of montmorillonite surface sites reactions (mainly de-protonation of $>S_{w1}OH$) to pH buffering in the buffer pore water.

The calculated maximum extent of montmorillonite dissolution is from initial 47 vol% to 43 vol% (at 10 000 years near buffer contact with the fracture – Fig. 8), and is not predicted to occur to an observable

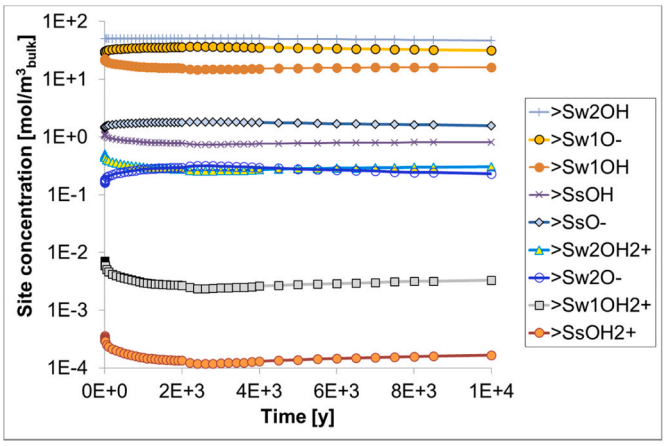

Fig. 7. *Base Case* composition of montmorillonite sorption sites at the observation point in the buffer near the fracture (see Fig. 4).

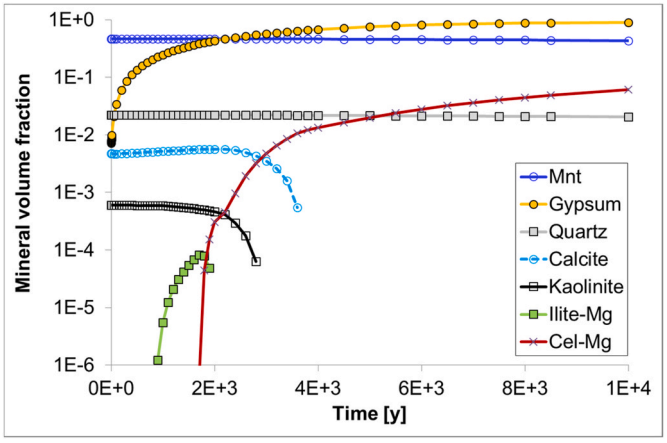

Fig. 8. *Base Case* volume changes of selected minerals at the observation point in the buffer near the fracture (see Fig. 4).

extent at the other observation points in the buffer (not shown). As shown in Fig. 8, changes in the content of other minerals are likewise expected to be limited, except for significant precipitation of gypsum. Gypsum precipitation in the bentonite buffer concentrates locally near the contact with the fracture and reaches values (0.9 vol fraction) that are in excess of the total porosity of the buffer (0.43), indicating the possibility for complete local porosity clogging.

Secondary mineral precipitation is predicted to occur also in the fracture due to mixing of the bentonite-derived fluids with the cement leachates. The mineral precipitation patterns vary in time and space within the fracture and are not shown here in detail. As an example, Fig. 9 presents the contents of selected minerals in the fracture along a profile away from the buffer/fracture interface at 10 000 years. The figure shows the formation of brucite, calcite, tobermorite and hydrotalcite as secondary phases in the fracture. In particular, the precipitation of brucite in the fracture is predicted to be locally extensive, reaching volume fractions (1.17) that are in excess of the total fracture porosity (unity). This indicates the potential for a localised fracture sealing.

3.2. Sensitivity cases

For simplicity, sensitivity cases are compared to the *Base Case* using maximum log10(change) of total components and maximum pH difference at the mid-buffer observation point during 10 000 years. Table 9 shows a comparison for all calculated cases, including the *Saline Ref* case.

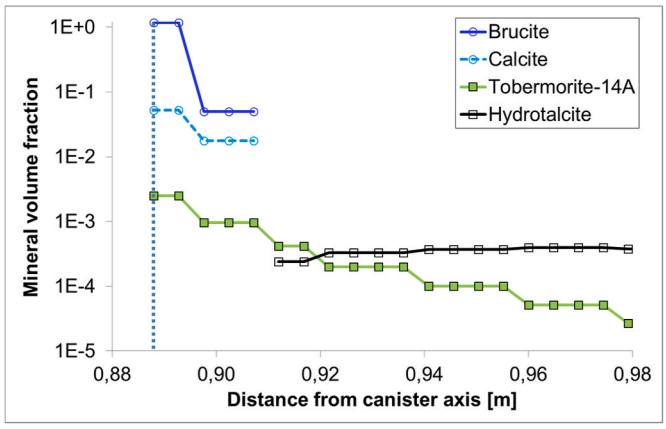

Fig. 9. *Base Case* mineral volume changes along a profile (at 10 000 years) away from the bentonite/fracture interface (indicated by the vertical dotted line) into the fracture, in the direction against leachate flow (see Fig. 4).

The results presented in Table 9 indicate that the fracture's aperture and the volumetric flow rate constitute an important constraint on the rate of solute mass transfer between the buffer porewater and the leachate in the fracture. Under slower advective flow, the mixing zone between the buffer porewater and leachate becomes broader and extends deeper into the fracture, away from the buffer; conversely, faster flow in the fracture tends to sharpen the mixing zone and move it towards the buffer (not shown). Higher aperture and flow in the *Frac High* case (aperture of 1 mm and average flow velocity of 10 [m/y]), leads to an increased extent of buffer porewater perturbation, especially for the weakly reacting components, such as chloride. At maximum log10 (change) of 0.75, chloride perturbation is almost identical to the "diffusive equilibrium" value of 0.76, indicating a near complete diffusive equilibration. Strongly reacting components are affected to a lesser extent. For example, the maximum pH difference during 10 000 years is calculated to be 0.09 unit, which is almost the same as in the *Base Case* (0.08 unit). On the other hand, a decreased flow rate (*Frac Low* case – 0.1 mm aperture and 1 m/y average flow velocity) is predicted to result in a consistently smaller extent of perturbation; notably, practically no pH change is expected in this case.

As discussed earlier, mineral precipitation reactions induced by cement leachate interactions with the porewater are expected to occur, especially near the buffer intersection with the leachate-bearing fracture, but are difficult to reliably quantify. Secondary mineral precipitation in the buffer and fracture due to interactions with cement leachates reduces porosity, which could decrease the rate of diffusive transport across the affected buffer zone. In this study, the potential effect of porosity reduction and its impact on diffusive transport is studied simplistically by assuming the presence of a ring-like buffer zone of reduced porosity along the fracture/buffer intersection trace line. The vertical and radial extent of this zone is assumed to be 1 cm, while the porosity is reduced to 10% (*Skin Poro 10%*) and 1% (*Skin Poro 1%*) from the *Base Case* value of 43%. Results shown in Table 9 indicate that porosity reduction due to mineral precipitation has a significant potential to reduce the extent of buffer porewater perturbation. In particular, in the case of porosity reduction down to 1%, the buffer is predicted to be practically "sealed-off" with no appreciable porewater change during 10 000 years.

To simplistically bound the uncertainty related to the *Base Case* effective diffusion coefficient, two sensitivity cases are considered: values three times higher (*High De*, $1.3 \cdot 10^{-10}$ [m^2/s]) and three times lower (*Low De*, $1.5 \cdot 10^{-11}$ [m^2/s]) than the *Base Case* value. Both of these cases yield results as expected: higher buffer diffusivity yields a higher extent of maximum porewater perturbation, while lower buffer diffusivity, *vice versa* (Table 9). Interestingly, the 3 times elevated diffusivity

Table 9
Comparison of maximum log10(change) of total components and maximum pH difference at the mid-buffer observation point during 10 000 years for all calculated cases. Refer to Table 7 for explanations on cases.

Total component	Saline Ref	Base Case	Frac High	Frac Low	Skin poro 10%	Skin poro 1%	De High	De Low	Mnt Rate Low	No Sec Min	pH 9.7	10% saline	50% saline	90% saline
	Maximum log10(Change) during 10 000 years at mid-buffer													
Cl	0.26	**0.56**	0.75	0.43	0.30	0.05	0.67	0.37	0.56	0.56	0.54	0.53	0.43	0.30
Ca	0.17	**0.48**	0.83	0.32	0.20	0.02	0.64	0.26	0.48	0.48	0.46	0.45	0.34	0.20
Mg	0.16	**0.44**	0.52	0.31	0.20	0.02	0.54	0.25	0.44	0.46	0.44	0.42	0.32	0.19
Na	0.09	**0.25**	0.33	0.17	0.11	0.01	0.31	0.14	0.25	0.25	0.24	0.23	0.17	0.11
K	0.09	**0.22**	0.23	0.17	0.11	0.01	0.28	0.13	0.22	0.25	0.24	0.19	0.18	0.11
Al	−0.01	**0.10**	0.12	0.03	0.06	−0.01	0.06	0.09	0.10	0.30	0.03	0.10	0.05	0.01
Si	−0.01	**−0.01**	−0.01	−0.01	−0.01	−0.01	−0.01	−0.01	−0.01	−0.01	−0.01	−0.01	−0.01	−0.01
S(VI)	−0.13	**−0.29**	−0.48	−0.21	−0.14	−0.02	−0.36	−0.18	−0.29	−0.29	−0.28	−0.27	−0.22	−0.15
C(IV)	−0.17	**−0.48**	−0.76	−0.32	−0.25	−0.03	−0.53	−0.33	−0.48	−0.68	−0.41	−0.48	−0.36	−0.21
	Maximum difference during 10 000 years at mid-buffer													
pH	−0.02	**0.08**	0.09	0.01	0.05	0.00	0.04	0.08	0.09	0.27	0.00	0.09	0.04	0.00

relative to the *Base Case* results in a smaller pH difference. This is explained by faster diffusive transport of dissolved carbonates from within the buffer (carbonate de-protonation reactions resist pH changes). Overall, the uncertainty in buffer diffusivity as bounded by the presented cases appears to be small.

The rate of montmorillonite dissolution in the buffer is uncertain. In this study, this uncertainty is bounded by considering a case where the *Base Case* montmorillonite rate constant is decreased 10 000 times (*Mnt Rate Low*). The maximum extent of buffer porewater perturbation in this case (Table 9) is identical to the *Base Case*, indicating that the contribution of montmorillonite dissolution to porewater buffering is negligible. This is consistent with the observed limited extent of montmorillonite dissolution discussed for the *Base Case*.

In a theoretical limiting case (*No Sec Min*), the precipitation rate of secondary clay and zeolite minerals was set to zero. The results of this case (Table 9) suggest that the precipitation of these minerals contributes considerably to buffering of pH and of Al, but has minor effect on other components. Overall, this case yields porewater pH perturbation with a maximum change of about 0.3 units during 10 000 years. Complete suppression of secondary clay and zeolite minerals during cement leachates reaction with bentonite porewater is unlikely, and this case should be considered unrealistically conservative. Despite this conservatism, the overall extent of porewater perturbation remains limited.

As discussed earlier, assuming a leachate composition corresponding to pH 11.6 throughout 10 000 years of the calculation can be seen as conservative. It is likely that the leachate composition will be characterised by a lower pH value due to extensive mixing with groundwater and mineral precipitation. Considering a composition corresponding to pH 9.7 is predicted to result in a maximum porewater composition change that is comparable to, or slightly lower than, that calculated for the *Base Case*. In particular, the pH is predicted to be completely neutralised by the buffer (except for a very small area directly contacting the fracture – not shown).

Cement leachates will undergo mixing with the groundwater during transport from the point of their generation towards the deposition hole. Progressive mixing and mineral precipitation will tend to shift the leachate's chemical composition towards that of the groundwater. In particular, pH of the leachate will decrease. Detailed modelling of leachate transport *via* the interconnected fracture network, mixing with the groundwater and the associated chemical reactions are beyond the scope of this study. Although not possible to quantify in this model, it is expected (Soler, 2010) that leachate mixing with the groundwater and mineral precipitation will significantly restrict the extent of the high-pH plume. To illustrate this qualitatively, three stylised cases (*10% Saline*, *50% Saline* and *90% Saline*) are considered. In these cases the effect of progressive leachate-groundwater mixing and mineral precipitation on the composition of the inflowing fluid, and its impact on the buffer porewater composition is simplistically represented. The results (Table 9) display a continuous transition from the *Base Case* towards the *Saline Ref* case with increasing degree of mixing. At 50% leachate mixing with the groundwater, the maximum porewater pH change is 0.04 unit, and the value tends towards null with further mixing.

4. Conclusions

Long-term predictive modelling of the potential impact of cement leachates on the chemical composition of the buffer porewater in the POSIVA disposal concept is challenging due to the complex nature of such interactions. Perturbation of buffer porewater composition varies depending on the component considered as well as time and location in the buffer. From repository safety point of view, the relevance of such perturbation depends on the impact it might have on the mobility (e.g. solubility, sorption and diffusion properties) of a specific radionuclide within the buffer.

Main modelling uncertainties include the composition of the leachates coming in contact with the buffer over time, the type and kinetic rate of induced mineral reactions, extent of porosity changes due to mineral reactions, and solute transport within the fracture and compacted bentonite. Although these processes cannot be quantified unequivocally, we demonstrate that it is possible to pessimistically bound their impact by a judicious choice of processes and parameter values.

Overall, the modelling results indicate that a combination of limited water flow within the fracture, slow diffusive exchange with the buffer, and mineral reactions will act together to minimise the extent of buffer porewater perturbation, should cement leachates reach the vicinity of a deposition hole. The *Base Case* model conservatively predicts a maximum porewater pH change to be less than 0.1 unit, except for a small area of the buffer directly adjacent to the fracture, where a maximum pH increase of 0.3 unit is predicted. Changes in the concentration of strongly reactive components, such as Al and Si, are expected to be negligible in most of the buffer volume. Perturbation of concentrations of major cations, such as Na^+, Ca^{2+}, Mg^{2+} and K^+, are predicted to be limited to a factor of 1.5–3 relative to their initial values, while the maximum change in the concentration of dissolved sulfate is predicted to be a factor of ca. 2, including near the contact with the fracture. Considering an additional level of conservatism on top of that already present in the *Base Case* (cases considering higher fracture aperture and flow rates, higher effective diffusivity of the buffer, no montmorillonite dissolution, or no precipitation of secondary minerals), could increase the *Base Case* perturbation values by no more than a further factor of ca. 2.

To put the *Base Case* results in context, it is useful to compare them with the reference scenario considering absence of cement leachates (*Ref Saline* case). The potential buffer porewater perturbation (concentration change) due to cement leachates is only about twice (or less) the magnitude expected to result from "natural" interactions with the groundwater, in absence of cement leachates.

On the other hand, cement leachate mixing with groundwater during

transport through the interconnected fracture network, and porosity reduction in the buffer due to mineral precipitation reactions, have the potential to cause a further significant reduction in buffer porewater perturbation. Although the impact of these processes is not possible to predict using the present model, they could reduce the magnitude of buffer porewater perturbation to a level comparable with values associated with the natural buffer porewater evolution.

As discussed, simplifications and generalisations had to be made during model development for computational efficiency reasons and due to lack of knowledge. The effect of some of these simplifications could be evaluated in a limiting or bracketing sense. For example, simplifications of model geometry (e.g. the spatial extent of the buffer and the exclusion of the bentonite backfill) tend to increase the extent of the buffer porewater chemical composition perturbation by the leachates. Some simplifications are difficult or impossible to quantify exactly. For example, ion transport in the compacted bentonite buffer is treated simplistically by considering a single porosity and a common diffusion coefficient to all ions. In view of conceptual and parametric uncertainties, and the computational burden associated with a more sophisticated treatment of ion transport in compacted clay, this approach is deemed justified.

The results of this study can serve as a basis for quantification of the maximum impact that cement leachates could have on the release and transport of radionuclides within the buffer. A comprehensive assessment is pending; however, based on previous experience, we expect this effect to be small relative to the overall uncertainty of the calculation.

Declaration of competing interest

The authors declare that they have no known competing financial interests or personal relationships that could have appeared to influence the work reported in this paper.

Acknowledgements

Financial support by POSIVA is acknowledged.

Two independent reviewers are thanked for their constructive comments and suggestions.

References

Bradbury, M.H., Baeyens, B., 1997. A mechanistic description of Ni and Zn sorption on Na-montmorillonite Part II: modelling. J. Contam. Hydrol. 27, 223–248.

Bradbury, M.H., Baeyens, B., 2003. Porewater chemistry in compacted re-saturated MX-80 bentonite. J. Contam. Hydrol. 61, 329–338.

De Windt, L., Marsal, F., Tinseau, E., Pellegrini, D., 2008. Reactive transport modeling of geochemical interactions at a concrete/argillite interface, Tournemire site (France). Phys. Chem. Earth 33, 295–305.

Fernández, R., Cuevas, J., Mäder, U., 2010. Modeling experimental results of diffusion of alkaline solutions through a compacted bentonite barrier. Cement Concr. Res. 40, 1255–1264.

Gaboreau, S., Prêt, D., Tinseau, E., Claret, F., Pellegrini, D., Stammose, S., 2011. 15 years of in situ cement–argillite interaction from Tournemire URL: characterisation of the multi-scale spatial heterogeneities of pore space evolution. Appl. Geochem. 26, 2159–2171.

Gaucher, E.C., Blanc, Ph, Matray, J.-M., Michau, N., 2004. Modeling diffusion of an alkaline plume in a clay barrier. Appl. Geochem. 19, 1505–1515.

Gaucher, E.C., Blanc, Ph, 2006. Cement/clay interactions – a review: experiments, natural analogues, and modeling. Waste Manag. 26, 776–788.

Giffaut, E., Grivé, M., Blanc, Ph, Vieillard, Ph, Colàs, E., Gailhanou, H., Gaboreau, S., Marty, N., Madé, B., Duro, L., 2014. Andra thermodynamic database for performance assessment: ThermoChimie. Appl. Geochem. 49, 225–236.

Hammond, G.E., Lichtner, P.C., Lu, C., Mills, R.T., 2012. PFLOTRAN: reactive flow and transport code for use on laptops to leadership-class supercomputers. In: Zhang, Fan, Yeh, G.T., Parker, Jack C. (Eds.), Groundwater Reactive Transport Models. Bentham Science Publishers, Sharjah, UAE, pp. 141–159, 2012.

Hammond, G.E., Lichtner, P.C., Mills, R.T., 2014. Evaluating the performance of parallel subsurface simulators: an illustrative example with PFLOTRAN. Water Resour. Res. 50, 208–228.

Hammond, G.E., Lichtner, P.C., Lu, C., Mills, R.T., 2019. PFLOTRAN: reactive flow & transport code for use on laptops to leadership-class supercomputers. In: Groundwater Reactive Transport Models, pp. 141–159. United States.

Hellä, P., Pitkänen, P., Löfman, J., Partamies, S., Vuorinen, U., Wersin, P., 2014. Safety Case for the Disposal of Spent Nuclear Fuel at Olkiluoto - Definition of Reference and Bounding Groundwaters, Buffer and Backfill Porewaters. *POSIVA Report* 2014-04.

Huertas, F.J., Chou, L., Wollast, R., 1998. Mechanism of kaolinite dissolution at room temperature and pressure: Part 1. Surface speciation. Geochem. Cosmochim. Acta 62, 417–431.

Juvankoski, M., 2017. Buffer System Description POS-014425. Bentoniittipuskurit, Järjestelmäkuvaus (POSIVA Internal Memorandum).

Kiviranta, L., Kumpulainen, S., Pintado, X., Kartuunen, P., Schatz, T., 2018. Characterization of Bentonite and Clay Materials 2012-2015. *POSIVA Working Report* WR 2016-05.

Koskinen, K., 2013. Effects of Cementitious Leachates on the EBS. *POSIVA Report* 2013-04.

Lehikoinen, J., 2009. Bentonite-cement interaction – preliminary results from model calculations. POSIVA Working Report 2009–2037.

Lüttge, A., Arvidson, R.S., Fischer, C., 2013. A stochastic treatment of crystal dissolution kinetics. Elements 9, 183–188.

Marty, N., Tournassat, Ch, Burnol, A., Giffaut, E., Gaucher, E.C., 2009. Influence of reaction kinetics and mesh refinement on the numerical modelling of concrete/clay interactions. J. Hydrol. 364, 58–72.

Marty, N., Claret, F., Lassin, A., Tremosa, J., Blanc, Ph, Made, B., Giffault, E., Cochepin, B., Tournassat, Ch, 2015. A database of dissolution and precipitation rates for clay-rocks minerals. Appl. Geochem. 55, 108–118.

Montori, J., Saaltink, M., Soler, P., 2008. Reactive transport modeling of the effect of hyperalkaline solutions along a fracture at the ONKALO site. POSIVA Working Report 2008–2014.

Parkhurst, D.L., Appelo, C.A.J., 2013. Description of input and examples for PHREEQC version 3 – a computer program for speciation, batch-reaction, one-dimensional transport, and inverse geochemical calculations: U.S. Geological Survey Techniques and Methods. book 6. http://pubs.usgs.gov/tm/06/a43. A43, 497.

Pfingsten, W., Paris, B., Soler, J.M., Mäder, U.K., 2006. Tracer and reactive transport modelling of the interaction between high-pH fluid and fractured rock: field and laboratory experiments. J. Geochem. Explor. 90, 95–113.

Pintado, X., Rautioaho, E., 2013. Thermo-Hydraulic Modelling of Buffer and Backfill. *POSIVA Report* 2012-48.

POSIVA, 2012a. Safety Case for the Disposal of Spent Nuclear Fuel at Olkiluoto – Synthesis 2012. *POSIVA Report* 2012-12.

POSIVA, 2012b. Safety Case for the Disposal of Spent Nuclear Fuel at Olkiluoto – Performance Assessment 2012. *POSIVA Report* 2012-04.

POSIVA, 2012c. Olkiluoto Site Description 2011. *POSIVA Report* 2011-02.

POSIVA, 2012d. Safety Case for the Disposal of Spent Nuclear Fuel at Olkiluoto – Assessment of Radionuclide Release Scenarios for the Repository System 2012. *POSIVA Report* 2012-09.

Read, D., Glasser, F.P., Ayora, C., Guardiola, M.T., Sneyers, A., 2001. Mineralogical and microstructural changes accompanying the interaction of Boom Clay with ordinary Portland cement. Adv. Cement Res. 13, 175–183.

Savage, D., Noy, D., Mihara, M., 2002. Modelling the interaction of bentonite with hyperalkaline fluids. Appl. Geochem. 17, 207–223.

Savage, D., Walker, C., Randy, A., Rochelle, Ch, Oda, C., Takase, H., 2007. Alteration of bentonite by hyperalkaline fluids: a review of the role of secondary minerals. Phys. Chem. Earth 32, 287–297.

Savage, D., Arthur, R., Watson, C., Wilson, J., Strömberg, B., 2011. Testing geochemical models of bentonite pore water evolution against laboratory experimental data. Phys. Chem. Earth 36, 1817–1829.

Steefel, C.I., Lichtner, P.C., 1998. Multicomponent reactive transport in discrete fractures II: infiltration of hyperalkaline groundwater at Maqarin, Jordan, a natural analogue site. J. Hydrol. 209, 200–224.

Soler, J.M., 2010. Reactive Transport Modeling of Grout-Rock Interaction at the ONKALO Site. *POSIVA Working Report* 2010-73.

Soler, J.M., 2011. Reactive transport modeling of grout-water interaction in a fracture at the ONKALO site effect of different potential groundwater compositions. POSIVA Working Report 2011–2083.

Soler, J.M., Vuorio, M., Hautojärvi, A., 2011. Reactive transport modeling of the interaction between water and a cementitious grout in a fractured rock. Application to ONKALO (Finland). Appl. Geochem. 26, 1115–1129.

Soler, J.M., 2012. High-pH plume from low-alkali-cement fracture grouting: reactive transport modeling and comparison with pH monitoring at ONKALO (Finland). Appl. Geochem. 27, 2096–2106.

Takase, H., 2004. Discussion on PA model development for bentonite barriers affected by chemical interaction with concrete: do we have enough evidence to support bentonite stability?. In: International Workshop on Bentonite-Cement Interaction in Repository Environments, pp. 172–177. Tokyo, Japan.

Velbel, M.A., 1990. Influence of temperature and mineral surface characteristics on feldspar weathering rates in natural and artificial systems: a first approximation. Water Resour. Res. 26, 3049–3053.

Vieno, T., Lehikoinen, J., Löfman, J., Nordman, H., Mészáros, F., 2003. Assessment of Disturbances Caused by Construction and Operation of ONKALO. *POSIVA Report* 2003-06.

Wersin, P., Kiczka, M., Rosch, D., 2014. Safety Case for a Spent Nuclear Fuel Repository at Olkiluoto: Radionuclide Solubility Limits and Migration Parameters for the Canister and Buffer. *POSIVA Report* 2012-39.

White, A.F., Brantley, S.L., 2003. The effect of time on the weathering of silicate minerals: why do weathering rates differ in the laboratory and field? Chem. Geol. 202, 479–506.

Zhu, C., 2005. In situ feldspar dissolution rates in an aquifer. Geochem. Cosmochim. Acta 69, 1435–1453.